

Article

# Modeling and Analysis of SOI Gratings-Based Opto-Fluidic Biosensor for Lab-on-a-Chip Applications <sup>†</sup>

Venkatesha Muniswamy <sup>1</sup>, Prasant Kumar Pattnaik <sup>2</sup> and Narayan Krishnaswamy <sup>1,\*</sup>

<sup>1</sup> Department of Electronics and Communication Engineering, Sai Vidya Institute of Technology, Bengaluru 560064, Karnataka, India; venkatesha.m@saividya.ac.in

<sup>2</sup> Department of Electrical and Electronics Engineering, BITS-Pilani, Hyderabad Campus, Hyderabad 500078, Telangana, India; pkpattnaik@hyderabad.bits-pilani.ac.in

\* Correspondence: narayank101@gmail.com; Tel.: +91-9980-893-447

<sup>†</sup> This paper is an extended version of our paper published in: Venkatesha, M.; Vismaya, K.R.; Prashanth, A.U.; Vyshnavi, M.; Narayan, K. Modeling and Analysis of SOI Grating Coupler for Bio-sensing Applications. In Proceedings of IEEE Photonics Conference (IPC), Reston, VA, USA, 30 September–4 October 2018.

Received: 20 May 2019; Accepted: 18 June 2019; Published: 20 June 2019



**Abstract:** The design, modeling, and analysis of a silicon-on-insulator (SOI) grating coupler integrated with a microfluidic channel for lab-on-a-chip applications are presented. The grating coupler was designed to operate at 1310 nm. The simulated SOI structure consisted of a 220 nm top-Si device layer with an integrated waveguide, grating coupler, and a buried oxide layer of 2  $\mu\text{m}$ . A rectangular microfluidic channel was deposited on the SOI optical grating structure for light and fluid interaction. The fluidic flow through the device was driven by centrifugal and Coriolis forces. The grating structure was designed to achieve a maximum coupling efficiency at the optimized injection angle of the light source. The sensitivity of the grating structure could be analyzed and evaluated using the change in coupled power as a function of the effective refractive index and was found to be  $0.928 \times 10^{-6}$  RIU. The SOI optical grating structure along with the micro fluidic channel on top could be effectively used as an absorbance-based lab-on-a-chip biosensor.

**Keywords:** lab-on-a-chip; grating; microfluidic channel; silicon-on-insulator

## 1. Introduction

Most bio-sensors are developed on silicon-on-insulator (SOI) substrates due to the high refractive index contrast between silicon device layers and buried oxide layers. Silicon is highly transparent in the infrared wavelength region of light, and therefore, silicon photonics has emerged as a promising solution for the development of opto-fluidic biosensors operating at the infrared wavelength region of light [1,2]. Low-loss photonic-integrated nanowires are developed on SOI substrates [3]. Recent developments in opto-fluidic-based biosensors have led to many sensors now being developed on SOI substrates, which include refractive index sensing and Bragg-grating-based sensors [2,4]. Integrated optical waveguides with gaps among them have shown great promise for sensing applications, including refractive index- and absorbance-based sensing [5–8].

Power coupling and light–fluidic interactions result in very interesting outcomes and are advancing state-of-the-art engineering and medical applications. One of the major challenges in optical waveguides is coupling of light between the optical source and the nanoscale waveguide [9–11]. One such efficient waveguide coupler that can couple light from the microscale to the nanoscale dimension is the fiber Bragg grating (FBG) coupler [12–16]. Fiber Bragg grating sensors have been developed for measuring

changes in physical parameters such as temperature, pressure, and magnetic field [17–21]. The Bragg wavelength for optical sensing applications is given by Equation (1) [22]:

$$\lambda_B = \frac{\Lambda \sin\theta}{m} \quad (1)$$

where  $\lambda_B$  is Bragg's wavelength,  $\Lambda$  is the grating pitch,  $m$  is an integer which indicates the order of diffraction, and  $\theta$  is the angle of incident light. In this article, the complete device was developed on an SOI substrate.

This article is an extended version of an earlier work entitled: "Modeling and Analysis of SOI Grating Coupler for Bio-Sensing Applications" [12]. In this work, a grating structure was designed on an SOI substrate having a 220 nm silicon device layer and a 2  $\mu\text{m}$  thick buried oxide (BOX) layer. In this structure, the coupling of light from the optical source to the nanoscale grating coupler was achieved by an optical lens. The injection angle greatly depends on the type of the optical source, which also affects the coupled power. In this work, the grating coupler was designed to operate over a broad frequency range. In the analysis of the grating coupler, a multi-frequency optical laser beam was used as an optical source resulting in a constant injection angle over a broad range of wavelengths. The analysis was conducted at a 1310 nm wavelength. This work focuses on optimizing the injection angle, determining the power coupling efficiency, and providing a comprehensive method for using such a structure for bio-sensing applications.

In Section 2.1, the proposed structure of the grating coupler (GC) sensor is discussed. Section 2.2 describes the simulation settings and design parameters. The simulation results for the injection angle and power coupled into the grating structure are discussed in Section 3. The results are validated with existing literature papers, after which bio-sensing applications for the device are discussed.

## 2. Materials and Methods

### 2.1. Structure and Design of Grating Coupler

The SOI GC was designed to operate at a wavelength of 1310 nm. The three-dimensional view of the SOI GC structure without the cladding region is shown in Figure 1. The bottom layer shown in red indicates the Si substrate. The middle region shown in green indicates the thin buried oxide (SiO<sub>2</sub>) layer and the top layer shown in dark red indicates a thin layer of Si, which consists of integrated waveguides and a grating structure. The grating structure is shown in Figure 2.

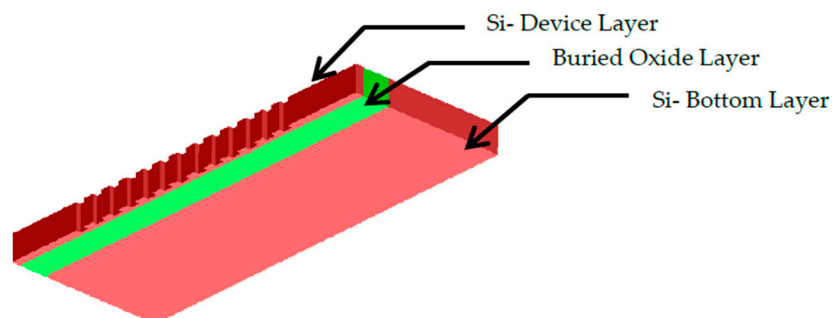


Figure 1. A 3D view of the silicon-on-insulator (SOI) grating structure.

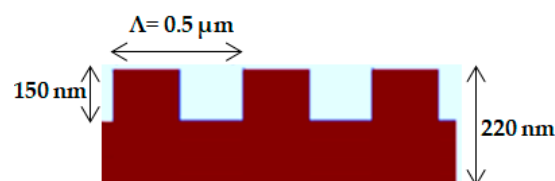


Figure 2. Grating structure dimensions.

The optimum injection angle,  $\theta$ , of the optical laser beam to maximize power coupling efficiency is calculated by Equation (2):

$$d = 1.37L_{gc}\cos\theta \tag{2}$$

where  $d$  represents beam diameter and  $L_{gc}$  is the grating coupler length. The grating pitch is provided by Equation (3):

$$\Lambda = \frac{2m\pi}{Kn_{eff} - \sin\theta} \tag{3}$$

where  $m$  represents the order of diffraction which is selected as 1 for first order diffraction,  $n_{eff}$  is the effective index of the complete SOI grating structure with a cladding layer, as shown in Figure 3,  $\theta$  is the optimum injection angle of the incident wave calculated from Equation (2), and  $K$  is the wave vector of the incident optical wave. At the selected wavelength of 1310 nm, the grating pitch ( $\Lambda$ ) for the proposed SOI-based grating coupler structure was calculated using Equation (3) and was found to be 0.5  $\mu\text{m}$ . Grating pitch and the Si-etch depth and Si-fill height are depicted in Figure 2.

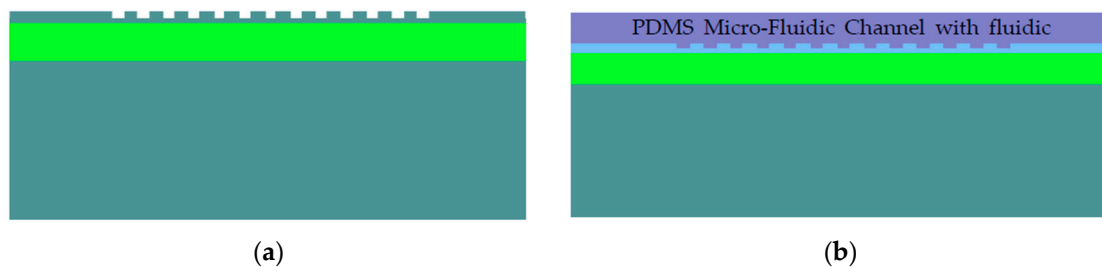


**Figure 3.** Front views of the SOI grating coupler: (a) without a PDMS microfluidic channel and (b) with a PDMS microfluidic channel.

Figure 3a,b show the front views of the SOI grating structure without and with cladding, respectively. During operation, the cladding layer acts as a microfluidic channel by having a complementary grating structure that can be filled with a fluidic sample. The complete details of the Polydimethylsiloxane (PDMS) microfluidic channel is discussed in Section 3.1. The presence of the fluid results in the absorption of optical power and the SOI grating structure can be used as an absorbance-based and refractive index-based lab-on-a-chip biosensor.

Table 1 gives the dimensions, materials, and the refractive index values used for the simulation analysis at a laser beam wavelength of 1310 nm. The grating pitch was calculated using Equation (3) for the optimum injection angle of 13.89 degrees obtained from Equation (2). The grating length,  $L_{gc}$  was 10  $\mu\text{m}$  and the laser beam diameter was 13.23  $\mu\text{m}$ .

**Table 1.** SOI grating coupler dimensions.

Parameter	Material	Dimensions in $\mu\text{m}$		Refractive Index
		Length	Height	N
Substrate	Silicon	10	2	3.47
Buried Oxide	SiO <sub>2</sub>	10	2	1.55
Input Waveguide	Silicon	2.5	0.22	3.47
Output Waveguide	Silicon	2.5	0.22	3.47
Grating Structure	Silicon	5	0.22	3.47

### 2.2. Simulation Settings

The simulations were carried out using the Lumerical mode solution and the Lumerical finite difference time domain (FDTD) simulation tools. A finite difference eigen (FDE) mode solver was used for the power coupling analysis. The FDE solver gives the spatial profile of the grating couple mode

(discussed in Section 3) at the wavelength of 1310 nm (Gaussian). The simulations were carried out for a single-frequency point and multiple-frequency point Gaussian beam sources.

In the simulation, the beam diameter was set to 13.23  $\mu\text{m}$  at a wavelength of 1310 nm and injected into a thin lens. A numerical aperture of 0.0265 was used for launching the light into the SOI grating structure.

The coupled power can be determined using Equation (4):

$$P_{\text{Coupled}} = P_{\text{Injected}} - (P_{\text{reflected}} + P_{\text{Transmitted}}) \quad (4)$$

The same approach was used in the simulation to calculate the coupled power. In the simulation, this method was reproduced by placing power monitors below and above the grating coupler to measure transmitted power and coupled power, respectively, and a third power monitor was placed at the end of the waveguide to directly measure coupled power.

The simulated SOI structure was optimized for maximum coupling efficiency at 1310 nm and it consisted of a 220 nm thick Si waveguide that was fabricated over a 1  $\mu\text{m}$  thick  $\text{SiO}_2$  layer. The coupling efficiency was determined for both single-beam and multi-beam optical sources and compared with the theoretical values shown in Section 3.

### 3. Results and Discussion

#### 3.1. Pressure along the Central Axis of the Channel

The structure (two-dimensional view) of the microfluidic PDMS channel is shown in Figure 4a. A lab-on-a-chip platform can be realized by designing a fluidic channel which is molded on the SOI grating coupler. The fluidic channel was 10  $\mu\text{m} \times 2\mu\text{m}$  in size. The center of the fluidic channel region consisted of the 0.5  $\mu\text{m}$  periodic structure having a height of 150 nm, which was molded on the SOI grating coupler. The schematic representation of the fluidic channel on the SOI grating is shown in Figure 4b.

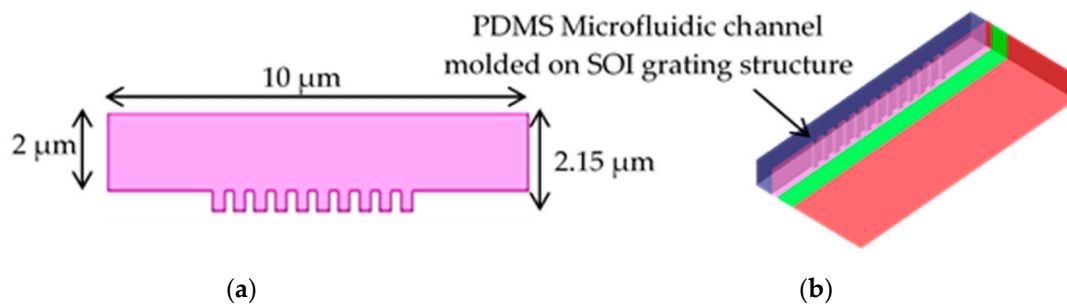


**Figure 4.** (a) The structure (two-dimensional view) of the PDMS microfluidic channel and (b) the SOI grating coupler with the PDMS microfluidic channel.

The nature of the fluidic sample considered in the analysis was whole blood with a density of 1060  $\text{Kg/m}^3$ , viscosity of  $3.5 \times 10^{-3}$  Pa.s. The mechanism of fluid flow manipulation in a rectangular fluidic channel depends on Coriolis or centrifugal forces. The Coriolis force acts along the length of the fluidic channel ( $y$ -axis). In a fluidic channel, the centrifugal force induces a parabolic flow profile pointing in the radial direction ( $z$ -axis). This is analogous to a pressure-driven flow.

Equation (5) provides the effective force acting on the fluidic sample injected into the channel. The effective force is equal to the sum of the centrifugal and Coriolis forces. Equations (6) and (7) gives the expressions of centrifugal and Coriolis forces respectively. The direction of the centrifugal force is in the radial direction ( $z$ -axis) of the fluidic channel.

$$F_{\text{effective}} = F_{\text{centrifugal}} + F_{\text{cor}} \quad (5)$$

$$\left| \vec{F}_{centrifugal} \right| = m\omega^2 r \quad (6)$$

$$\left| \vec{F}_{cor} \right| = 2m\omega(v_y - v_z) \quad (7)$$

The velocity-dependent Coriolis force produces an inhomogeneous transverse force in the tangential direction, which has its highest value in the center of the channel. The pressure acting on the rectangular fluidic channel, having dimensions of  $10 \mu\text{m} \times 2 \mu\text{m}$ , was simulated using the computational fluid dynamics (CFD) module in the COMSOL MULTYPHYSICS simulation tool. Figure 5 shows the pressure along the channel axis. The Coriolis force acting at the inlet implied that there should be a pressure gradient in the y-direction. There is a pressure perpendicular to the flow when gravity acts in the perpendicular direction, so pressure gradients in the y-direction will be produced by the Coriolis force. Therefore, the fluidic flow through the device was a result of centrifugal and Coriolis forces. The total flow rate through the channel was  $15.6 \mu\text{L/s}$ . The fluid flow was laminar and the highest velocity was found at the central axis of the device with parabolic flow.

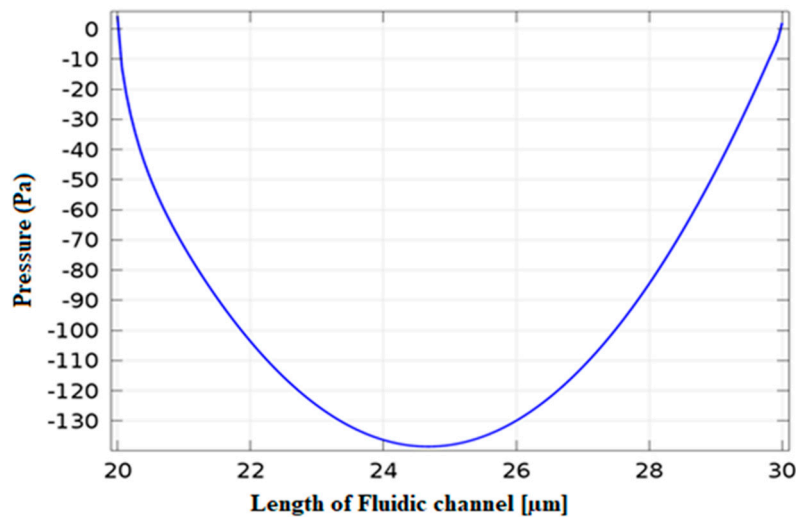


Figure 5. Pressure along the central axis of the channel.

### 3.2. Power Coupling Analysis

The coupled power from the integrated SOI input waveguide to the SOI output waveguide through the grating coupler, which was present below the sensing layer as shown in Figure 3, was simulated by using finite difference time domain simulation methods at a wavelength of 1310 nm using an indirect method (Method 1) and a direct method (Method 2). In the simulation, the PDMS microfluidic channel with whole blood was considered as a refractive index layer having a refractive index of 1.334 which was the refractive index of whole blood.

In Method 1, the coupled power was calculated by subtracting the injected power from the power calculated by Monitor 1 and Monitor 2, which were used to calculate transmitted power and reflected power, respectively. In Method 2, the coupled power was directly measured by a third power monitor placed at the end of the waveguide.

Figure 6 shows a combined plot of coupled power from both methods as a function of wavelength. It shows that the maximum coupled power was achieved for a wavelength of 1310 nm for both the indirect method as well as the direct method. At this wavelength, the maximum coupling efficiency was found to be  $\sim 55.2\%$  for the indirect method as well as the direct method.

The coupled power reported in this paper agrees with the results reported ( $55.7\%$ ) in the work conducted by Vivien et al. [22] involving light injection in SOI micro-waveguides using high-efficiency grating couplers.

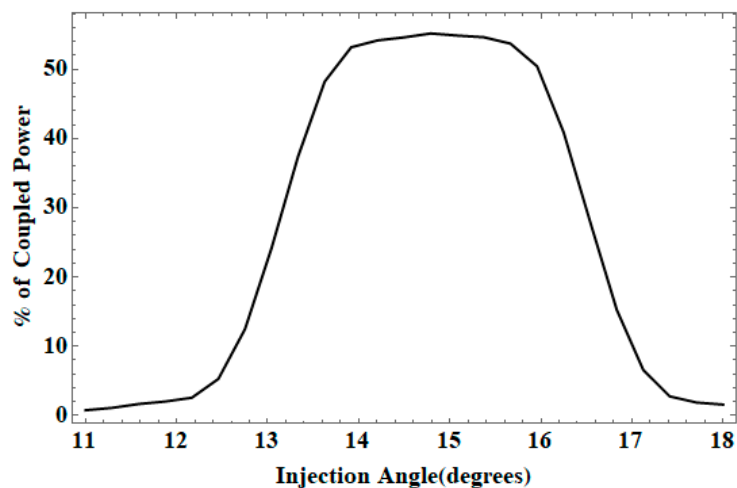


**Figure 6.** Injection angle as a function of coupled power.

Power coupling as a function of injection angle sweep analysis was carried out to optimize the injection angle  $\theta$  and to achieve maximum coupling efficiency. The maximum coupled power of  $\sim 55.2\%$ , as shown in Figure 6, was achieved at an injection angle of 14.1 degrees. The coupled power was almost constant at 55.2% for the injection angle from 13.5 degrees to 16 degrees. Therefore, for a broad range of wavelength it is possible to choose a constant injection angle anywhere from 13.5 degrees to 16 degrees. The coupled power as a function of wavelength is shown in Figure 7. The coupled power was maximum at a wavelength of  $\sim 1310$  nm. The simulated result obtained was in close agreement with the theoretical value of 13.9 degrees reported by Viven et al. [22].

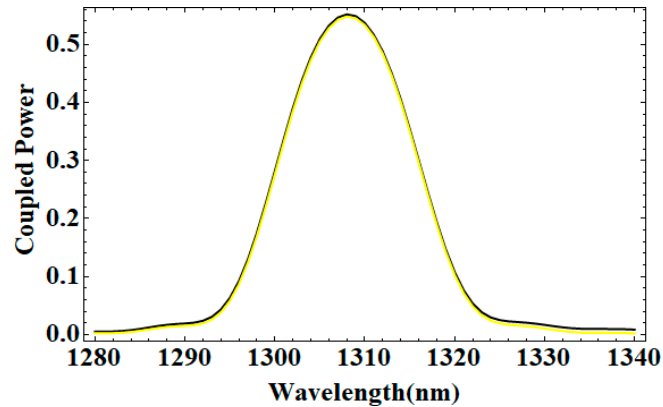


**Figure 7.** Combined coupled power plots using the direct method (shown in yellow) and the indirect method (shown in black) as a function of wavelength.

The refractive index of the fluidic sample injected into the PDMS microfluidic channel was 1.334 during simulation. This is close to the refractive index of biological samples such as hemoglobin present in human blood. The optical gratings were illuminated by a laser of wavelength 1310 nm and a part of the reflected as well as coupled power was absorbed by the microfluidic sample (in this paper, a cladding region with a refractive index of 1.334 was used). As a result of the absorption by the sample, the coupled power was reduced. This change in coupled power due to the absorption of transmitted and coupled power by the fluidic sample altered the effective index of the entire SOI grating coupler biosensor. The variation in effective index as a function of wavelength is shown in Figure 8. The effective index at an operating wavelength of 1310 nm was found to be approximately equal to 2.806.

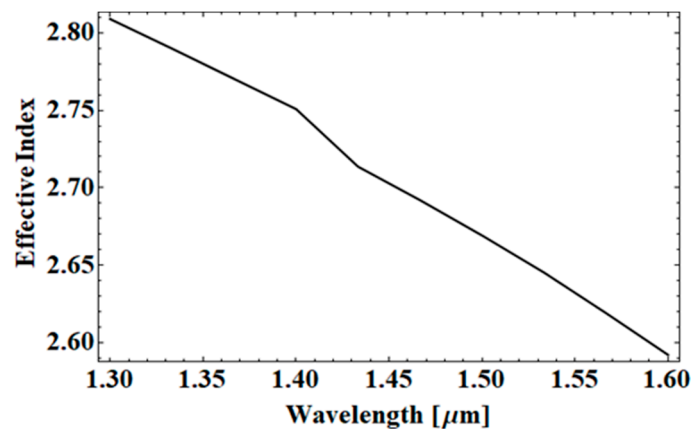


Figure 8. Effective index as a function of wavelength.

The sensitivity of the SOI grating coupling coupler was determined using Equation (8):

$$S = \frac{\partial P_{\text{coupled}}}{\partial n_{\text{eff}}} \quad (8)$$

where  $\partial P_{\text{coupled}}$  is the variation in coupled power and  $\partial n_{\text{eff}}$  is the variation in the effective index. The sensitivity was found to be  $0.928 \times 10^{-6}$  RIU. Such sensors, if fabricated, can be effectively used as lab-on-chip biosensors [23]. Such SOI gratings coupled with a microfluidic channel can be effectively used as absorbance-based and refractive index-based biosensors for point-of-care diagnostics.

### 3.3. Proposed Fabrication Steps

The fabrication process flow steps of the SOI waveguide structure was simulated using Intellisense (version 8.9, Lynnfield, MA, USA) and is shown in Figure 9. The fabrication process flow steps for an SOI gratings sensor without a PDMS microfluidic channel involves the following steps.

1. SOI wafer definition with a 1 μm thick buried oxide, substrate thickness (bottom Si) 2 μm, and top Si-device layer thickness 220 nm;
2. Deposition of 220 nm PR-AZ5214 photoresist using spin coating;
3. UV lithography, layer 1 of mask (waveguide region) is exposed to UV to leave photoresist inside. Layer 1 is a positive mask;
4. Etch Si by reactive ion etching (RIE, Cl<sub>2</sub>/CF<sub>4</sub>), etch thickness 200 nm (etch through);
5. UV lithography, layer 2 of mask (gratings between waveguides) is exposed to UV to leave photoresist outside. Layer 2 is a negative mask;
6. Etch Si by RIE (Cl<sub>2</sub>/CF<sub>4</sub>), etch thickness 150 nm (partial etch);
7. Etch PR-AZ5214, lift-off 220 nm thick PR-AZ5214.

The complete integrated opto-fluidic SOI gratings sensor shown in Figure 4 can be achieved by depositing the PDMS microfluidic channel on the SOI optical gratings sensor as referenced in the last process step, Etch PR-AZ5214, lift-off 220 nm thick PR-AZ5214, and shown in Figure 9. Such an opto-fluidic SOI gratings sensor can be used as an absorbance and refractive index-based lab-on-a-chip biosensor.

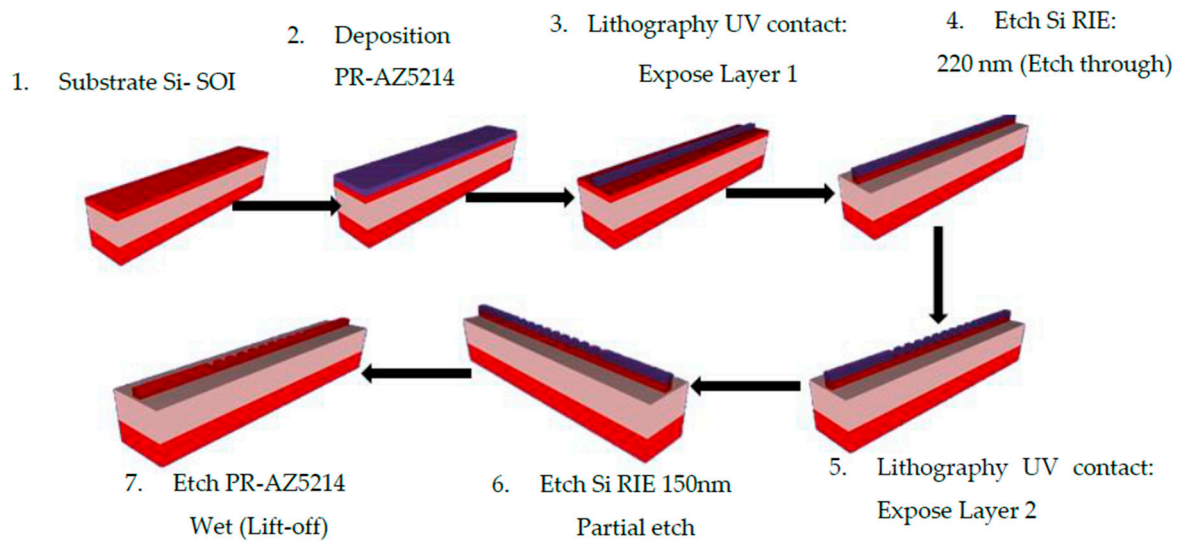


**Figure 9.** Fabrication process flow steps of the SOI grating coupler simulated using the Intellisense simulation package.

#### 4. Conclusions

In this work, the simulation and modeling of an SOI grating coupler integrated with a microfluidic channel operating at 1310 nm was presented. The flow through the device was a result of centrifugal and Coriolis forces. The total flow rate through the channel was 15.6  $\mu\text{L/s}$ . The grating coupler was analyzed for coupling power and optimum injection angle. The grating structure was designed to achieve maximum coupling efficiency. In the characterization of the grating structure, the coupled power was analyzed for a broad range of wavelengths and the injected angle was optimized for maximum coupling power. A maximum coupled power of  $\sim 55.2\%$  was achieved for an injection of 14.1 degrees. The effective index was found to be 2.806 for an SOI grating coupler having a cladding with a refractive index of 1.334. The maximum sensitivity was found to be  $0.928 \times 10^{-6}$  RIU which is in close agreement with the sensitivity reported in the work carried out by Dwivedi et al. [3] on refractive index sensing using silicon on insulator waveguide-based directional coupler. This work also suggested a fabrication method for using such SOI grating structures for lab-on-a-chip bio-sensing applications.

**Author Contributions:** Conceptualization, V.M. and N.K.; Methodology, V.M.; Software, V.M. and N.K.; Validation, V.M., P.K.P. and N.K.; Formal Analysis, V.M.; Investigation, V.M.; Resources, N.K.; Data Curation, V.M.; Writing-Original Draft Preparation, V.M.; Writing-Review & Editing, N.K. and P.K.P.; Visualization, V.M.; Supervision, N.K.; Project Administration, N.K.

**Funding:** This research was funded by the Department of Science and Technology, Science and Engineering Research Board (DST-SERB), Government of India, grant number YSS/2015/000382.

**Acknowledgments:** The authors would like to thank the Department of Science and Technology, Science and Engineering Research Board (DST-SERB), Government of India, Grant No. YSS/2015/000382, for funding this research work.

**Conflicts of Interest:** The authors declare no conflict of interest.

#### References

1. Lipson, M. Guiding, modulating and emitting light on silicon—Challenges and opportunities. *J. Lightwave Technol.* **2005**, *23*, 4222–4238. [[CrossRef](#)]
2. Luan, E.; Shoman, H.; Ratner, D.M.; Cheung, K.C.; Chrostowski, L. Silicon Photonic Biosensors Using Label-Free Detection. *Sensors* **2018**, *18*, 3519. [[CrossRef](#)] [[PubMed](#)]
3. Dwivedi, R.; Kumar, A. Refractive index sensing using silicon-on-insulator waveguide based modal interferometer. *Optik* **2018**, *156*, 961–967. [[CrossRef](#)]

4. Gnan, M.; Thorns, S.; Macintyre, D.S.; De La Rue, R.M.; Sorel, M. Fabrication of low-loss photonic wires in silicon-on-insulator using hydrogen silsesquioxane electron-beam resist. *Electron. Lett.* **2008**, *44*, 115–116. [[CrossRef](#)]
5. Komljenovic, T.; Huang, D.; Pintos, P.; Tran, M.A.; Davenport, M.L.; Bowers, J.E. Photonic Integrated Circuits Using Heterogeneous Integration on Silicon. *Proc. IEEE* **2018**, *106*, 2246–2257. [[CrossRef](#)]
6. Shwetha, M.; Kumar, M.; Narayan, K. Modeling and simulation of opto-fluidic based Mach-Zehnder interferometer for biosensing application. In Proceedings of the Workshop on Recent Advances in Photonics (WRAP), Bangalore, India, 16–17 December 2015.
7. Miller, D.A.B. Rationale and challenges for optical interconnects to electronic chips. *Proc. IEEE* **2000**, *88*, 728–749. [[CrossRef](#)]
8. Sridaran, S.; Bhave, S.A. Nanophotonic devices on thin buried oxide Silicon-On-Insulator substrates. *Opt. Express* **2010**, *18*, 3850–3857. [[CrossRef](#)] [[PubMed](#)]
9. Zaoui, W.S.; Kunze, A.; Vogel, W.; Berroth, M.; Butschke, J.; Letzkus, F.; Burghartz, J. Bridging the gap between optical fibers and silicon photonic integrated circuits. *Opt. Express* **2014**, *22*, 1277–1286. [[CrossRef](#)] [[PubMed](#)]
10. Shiraishi, K.; Yoda, H.; Ohshima, A.; Ikeda, H.; Tsai, C.S. A silicon-based spot-size converter between single-mode fibers and Si-wire waveguides using cascaded tapers. *Appl. Phys. Lett.* **2007**, *91*, 141120. [[CrossRef](#)]
11. Luyssaert, B.; Bienstman, P.; Vandersteegen, P.; Dumon, P.; Baets, R. Efficient non-adiabatic planar waveguide tapers. *J. Lightwave Technol.* **2005**, *23*, 2462–2468. [[CrossRef](#)]
12. Venkatesha, M.; Vismaya, K.R.; Prashanth, A.U.; Vyshnavi, M.; Narayan, K. Modeling and Analysis of SOI Grating Coupler for Bio-sensing Applications. In Proceedings of the 2018 IEEE Photonics Conference (IPC), Reston, VA, USA, 30 September–4 October 2018; pp. 1–2.
13. Sethi, P.; Haldar, A.; Selvaraja, S. Ultra-compact low-loss broadband waveguide taper in silicon-on-insulator. *Opt. Express* **2017**, *25*, 10196–10203. [[CrossRef](#)]
14. Chen, D.; Xiao, X.; Wang, L.; Yu, Y.; Liu, W.; Yang, Q. Low-loss and fabrication tolerant silicon mode-order converters based on novel compact tapers. *Opt. Express* **2015**, *23*, 11152–11159. [[CrossRef](#)] [[PubMed](#)]
15. Ding, Y.; Ou, H.; Peucheret, C. Ultrahigh-efficiency apodized grating coupler using fully etched photonic crystals. *Opt. Lett.* **2013**, *38*, 2732–2734. [[CrossRef](#)] [[PubMed](#)]
16. Ma, Y.; Zhang, Y.; Yang, S.; Novack, A.; Ding, R.; Lim, A.E.-J.; Lo, G.-Q.; Baehr-Jones, T.; Hochberg, M. Ultralow loss single layer submicron silicon waveguide crossing for SOI optical interconnect. *Opt. Express* **2013**, *21*, 29374–29382. [[CrossRef](#)] [[PubMed](#)]
17. Rao, Y.J. Fiber Bragg grating sensors: Principles and applications. In *Optical Fiber Sensor Technology. Optoelectronics, Imaging and Sensing*; Grattan, K.T.V., Meggitt, B.T., Eds.; Springer: Boston, MA, USA, 1998; Volume 2, ISBN 978-1-4613-7651-4.
18. Errando-Herranz, C.; Colangelo, M.; Ahmed, S.; Björk, J.; Gylfason, K.B. MEMS tunable silicon photonic grating coupler for post-assembly optimization of fiber-to-chip coupling. In Proceedings of the 2017 IEEE 30th International Conference on Micro Electro Mechanical Systems (MEMS), Las Vegas, NV, USA, 22–26 January 2017; pp. 293–296.
19. Kim, J.H.; Park, J.H.; Han, S.K.; Bae, M.J.; Yoo, D.E.; Lee, D.W.; Park, H.H. Tunable Grating Couplers for Broadband Operation Using Thermo-Optic Effect in Silicon. *IEEE Photonics Technol. Lett.* **2015**, *27*, 2304–2307. [[CrossRef](#)]
20. Galan, J.V.; Sanchis, P.; Blasco, J.; Marti, J. Study of High Efficiency Grating Couplers for Silicon-Based Horizontal Slot Waveguides. *IEEE Photonics Technol. Lett.* **2008**, *20*, 985–987. [[CrossRef](#)]
21. Pollock, C.R. *Fundamentals of Optoelectronics*; Irwin: Chicago, IL, USA, 1995; ISBN 978-0-256-10104-1.
22. Vivien, L.; Pascal, D.; Lardenois, S.; Marris-Morini, D.; Cassan, E.; Grillot, F.; Laval, S.; Fédéli, J.-M.; El Melhaoui, L. Light injection in SOI micro-waveguides using high-efficiency grating couplers. *J. Lightwave Technol.* **2006**, *24*, 3810–3815. [[CrossRef](#)]
23. Venkatesha, M.; Chaya, B.M.; Pattnaik, P.K.; Narayan, K. Modeling and Analysis of an Opto-Fluidic Sensor for Lab-on-a-Chip Applications. *Micromachines* **2018**, *9*, 134.

